



HAL
open science

Original Layered OP₄-(Li,Na) x CoO₂ Phase: Insights on Its Structure, Electronic Structure, and Dynamics from Solid State NMR

Yohan Biecher, Danielle L. Smiley, Marie Guignard, François Fauth, Romain Berthelot, Claude Delmas, Gillian R. Goward, Dany Carlier

► **To cite this version:**

Yohan Biecher, Danielle L. Smiley, Marie Guignard, François Fauth, Romain Berthelot, et al.. Original Layered OP₄-(Li,Na) x CoO₂ Phase: Insights on Its Structure, Electronic Structure, and Dynamics from Solid State NMR. *Inorganic Chemistry*, 2020, 59 (8), pp.5339-5349. 10.1021/acs.inorgchem.9b03417 . hal-02569531

HAL Id: hal-02569531

<https://hal.science/hal-02569531>

Submitted on 11 May 2020

HAL is a multi-disciplinary open access archive for the deposit and dissemination of scientific research documents, whether they are published or not. The documents may come from teaching and research institutions in France or abroad, or from public or private research centers.

L'archive ouverte pluridisciplinaire **HAL**, est destinée au dépôt et à la diffusion de documents scientifiques de niveau recherche, publiés ou non, émanant des établissements d'enseignement et de recherche français ou étrangers, des laboratoires publics ou privés.

On the original layered OP4-(Li,Na)_xCoO₂ phase : insights on its structure, electronic structure and dynamics from solid state NMR

*Yohan Biecher^a, Danielle L. Smiley^b, Marie Guignard^a, François Fauth^c, Romain Berthelot^{d,e},
Claude Delmas^a, Gillian R. Goward^b, Dany Carlier^{a,e,*}*

^aCNRS, Univ. Bordeaux, Bordeaux INP, ICMCB UMR 5026, F-33600 Pessac, France

^bDepartment of Chemistry & Chemical Biology, McMaster University, Hamilton, Ontario L8S 4M1, Canada

^cCELLS - ALBA synchrotron, Cerdanyola del Vallès, E-08290 Barcelona, Spain

^dCNRS, Univ. Montpellier, ICGM UMR 5253, F-34095 Montpellier, France ICGM, Université de Montpellier, CNRS, 34095 Montpellier, France

^eRéseau sur le Stockage Electrochimique de l'Énergie (RS2E), CNRS, 80039 Amiens, France

* *Corresponding author:* dany.carlier@icmcb.cnrs.fr

Abstract: The OP4-(Li/Na)_xCoO₂ phase is an unusual lamellar oxide with a 1:1 alternation between Li and Na interslab spaces. In order to probe the local structure, electronic structure and dynamics, ⁷Li and ²³Na magic angle spinning nuclear magnetic resonance (MAS NMR) spectroscopy were performed in complementarity to X-ray diffraction and electronic and magnetic properties measurements. ⁷Li MAS NMR showed that NMR shifts result from two contributions: the Fermi contact and the Knight shifts due to the presence of both localized and delocalized electrons that is really unusual. ⁷Li MAS NMR clearly shows several Li environments indicating that, moreover, Co ions with different local electronic structures are formed, probably due to the arrangement of the Na⁺ ions in the next cationic layer. ²³Na MAS NMR showed that some Na⁺ ions are located in the Li layer what was not previously considered in the structural model. The Rietveld refinement of the synchrotron XRD led to the OP4-[Li_{0.42}Na_{0.05}]Na_{0.32}CoO₂ formula for the material. In addition, ⁷Li and ²³Na MAS NMR provide information about the cationic mobility in the material: whereas no exchange is observed for ⁷Li up to 450K, the ²³Na spectra reveals already a single average signal at room temperature due to much larger ionic mobility.

1. Introduction

The layered structure of A_xMO_2 (A = alkaline ion, M = transition metal ion) phases is at the origin of a wide range of peculiar properties, such as electrochemical energy storage in Li-ion or Na-ion batteries^{1,2}, thermoelectric properties^{3,4}, superconductivity⁵⁻⁷. These lamellar oxides consist of a stacking of edge-sharing MO_6 octahedra layers forming MO_2 slabs between which alkali A^+ ions are intercalated. Delmas *et al.* introduced in 1980 a specific nomenclature composed by a letter and a number indicating, respectively, the alkaline site geometry and the number of layers necessary to describe the structure in the hexagonal cell⁸. Indeed, different types of interstitial sites are reported in the literature depending on the nature of the alkali ion A^+ , its concentration x and the synthesis conditions⁹: Octahedral (for example O3-LiCoO₂¹⁰), Tetrahedral¹¹ or Prismatic (for example P2-Na_xCoO₂ or P3-Na_xCoO₂¹²).

In this paper, we were interested in a unique (Li/Na) mixed lamellar oxide with Na and Li layers alternating along the c axis, first reported in 1994 by Balsys and Davis¹³. As this material was initially synthesized from the layered O3-LiCoO₂ and P2-Na_{0.7}CoO₂ phases as precursors with a 1:1 molar ratio, the Li_{0.5}Na_{0.35}CoO₂ ideal formula would have been expected. However, the LiCoO₂ is present as product from such a stoichiometric mixture of precursors. Actually, a Li_{0.43}Na_{0.36}CoO_{1.96} phase composition was deduced from a Rietveld refinement of the neutron diffraction data¹³. The structure of the phase is formed by edge-sharing CoO₆ octahedra layers with interslab spaces alternatively occupied by Na⁺ and Li⁺ ions, as shown in **Figure 1**. The alkali ions keep the intercalation site symmetry of the precursors, *i.e.* octahedral and trigonal prismatic for the lithium and sodium ions respectively, thus forming an OP4 stacking. Note that there are two prismatic intercalation sites for Na⁺ ions, one sharing the faces (Na_f) and the other sharing the edges (Na_e) with the surrounding CoO₆ octahedra as in P2-Na_xCoO₂¹⁴ (**Figure 1a and 1b**). By using O3-

LiCoO₂ and P2-Na_{0.7}CoO₂ as precursors for their synthesis, Balsys and Davis indicated the difficulty to obtain a pure phase.

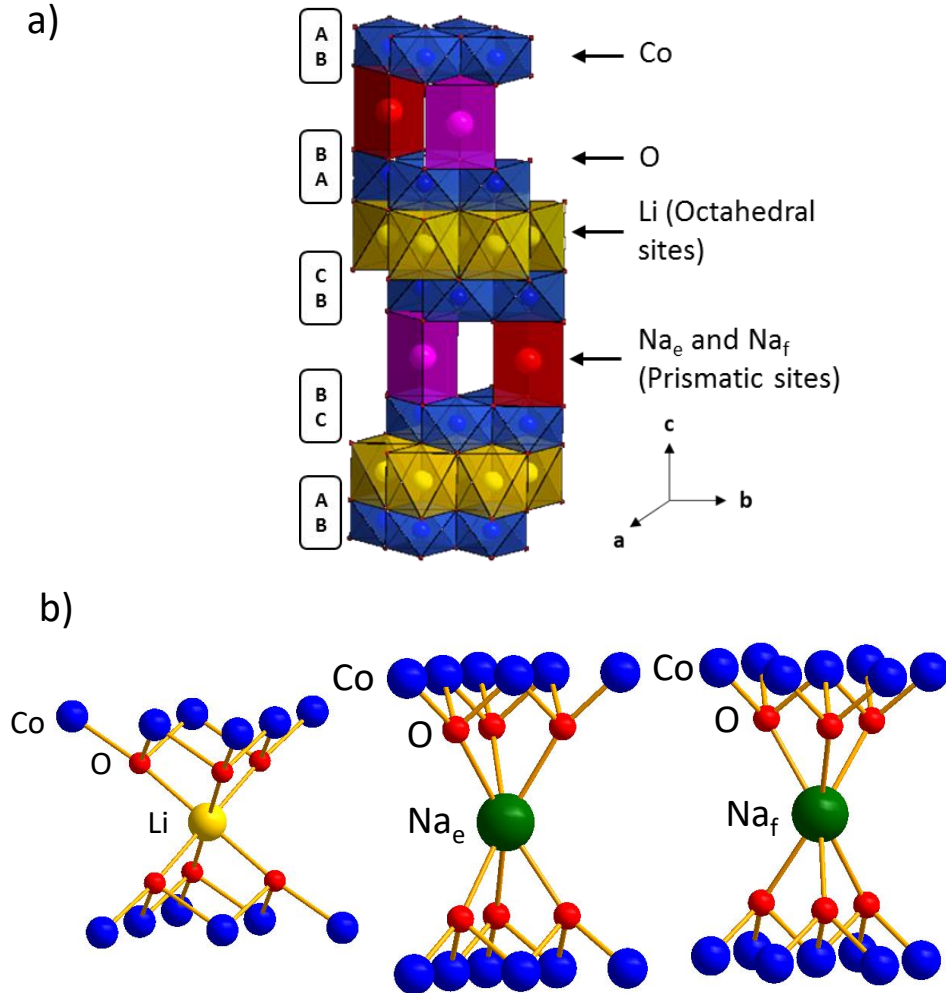


Figure 1: a) Perspective representation of the OP4-(Li/Na)CoO₂ phase and b) local Li and Na environments : Li⁺ ions occupy octahedral sites sharing edges with CoO₆ and the Na⁺ ions occupy prismatic sites which can either share faces (Na_f) or edges (Na_e) with CoO₆ octahedra.

Additional publications propose the synthesis of this phase without any consensus concerning the best precursors or thermal treatment to obtain the purest phase¹⁵⁻²¹. Table in **SI-1** summarizes the chemical compositions and cell parameters reported in the literature for the OP4 phase. All the

proposed chemical formulas differ from the ideal $\text{Li}_{0.5}\text{Na}_{0.35}\text{CoO}_2$ one, but the presence of traces of O3- LiCoO_2 and P2- $\text{Na}_{0.7}\text{CoO}_2$ as impurities may alter the composition determined by Inductively Coupled Plasma (ICP) measurements¹⁷. Some of us, for the first time, studied the formation of the OP4- $(\text{Li,Na})_x\text{CoO}_2$ phase by *in situ* variable temperature X-Ray Diffraction (XRD): the phase is formed at around 855°C but decomposes back into O3- LiCoO_2 and P2- $\text{Na}_{0.7}\text{CoO}_2$ if slowly cooled¹⁸. Since the layered OP4 phase is really original in solid-state chemistry and might exhibit peculiar properties, especially because of a different occupation ratio of the alkaline layers, we decided to investigate further its structure, electronic structure and alkaline ions dynamics, using Magic Angle Spinning Nuclear Magnetic Resonance (MAS NMR) spectroscopy as a local probe.

Indeed, ^7Li MAS NMR has been shown to be a powerful probe to characterize both the structural and electronic local environments in paramagnetic materials²². The latter can be deduced from the MAS NMR studies thanks to the hyperfine interactions (electron spin-nucleus spin coupling). In paramagnetic compounds, as in the case of most of the positive electrode materials, the spectra are dominated by the Fermi contact interactions, leading to the following shift:

$$\delta_{Fermi}^i(T) = \frac{1}{3SN_A} \rho^i(0) \chi_M(T) \quad \text{eq. (1)}$$

where S is the spin quantum number of the paramagnetic ion, $\rho^i(0)$ is the spin density on the i nucleus and χ_M the molar magnetic susceptibility (at the temperature of the NMR measurement). The interpretation of the Fermi contact shift interactions can be supported by DFT calculations with the aim to assign the different signals^{23–31} and understand the spin transfer mechanisms reflecting the local electronic structure^{23,29–31}. In metallic compounds, the spectra are dominated by the Knight shift:

$$\delta_{Knight} = \frac{8\pi}{3} \langle |\psi_{r=0}|^2 \rangle \chi_s^e \quad \text{eq. (2)}$$

where χ_s^e is the Pauli susceptibility of conduction bands electrons at Fermi level and $\langle |\psi_{r=0}|^2 \rangle$ is the contribution of “s” orbitals at Fermi level of probed nucleus.

In addition, solid state NMR can be also used to probe the alkaline ions mobility in electrode materials (exchange spectroscopy³²⁻³⁴, variable-temperature³³ (VT), rotational-echo double-resonance³⁵ or selective inversion³⁶ for instance).

In this paper, we report a ⁷Li and ²³Na MAS NMR study of several OP4 phases to investigate the local structure, electronic structure and the dynamics in complementarity to X-Ray Diffraction (XRD) and electronic/magnetic properties measurements.

2. Experimental

Synthesis

The syntheses were performed using either alkaline carbonates and Co₃O₄, or O3-LiCoO₂ and P2-Na_{~0.7}CoO₂ as precursors. As less impurities were observed by XRD with the first set of precursors, we report here only syntheses carried on using Li₂CO₃ (Sigma-Aldrich, 99.9%, dried at 350°C), Na₂CO₃ (Sigma Aldrich, 99.9%, dried at 200°C) and Co₃O₄ (home-made from cobalt nitrate, heat treated under air at 450°C). Those precursors were initially mixed and ground together in an Ar-filled glovebox targeting 1g of OP4 phase. Slightly different chemical compositions around Li_{0.42}Na_{0.38}CoO₂¹⁸ were used in order to compensate possible alkaline ion loss by evaporation during the heat treatment. Three samples were selected here and labelled A, B and C.

Their initial compositions are summarized in **Table 1**. The powders were then pressed into pellets in a controlled argon atmosphere and the pellets were heated in a furnace under air at 870 °C for 48 h with a 2°C/min heating rate. After the heat treatment, all the pellets were rapidly quenched to room temperature and entered in the Ar-filled glovebox again.

	Initial alkaline content for a $\text{Li}_x\text{Na}_y\text{CoO}_2$ composition	
	x	y
Sample C	0.42	0.40
Sample B	0.42	0.41
Sample A	0.44	0.38

Table 1: Initial alkaline compositions in the precursors mixture of the three selected OP4 samples labelled: A, B and C.

Characterizations

SEM : Scanning electron microscopy images were taken using a Hitachi S-4500 microscope. SEM pictures show primary particles with a typical hexagonal shape with around 3 µm in diameter and 0.5 µm in thickness (**Figure S2**) for the synthesized compounds.

XRD: Angular resolution synchrotron X-Ray powder diffraction (SXRPD) experiments were performed at room temperature on the BL04-MSPD beamline of the ALBA synchrotron (Cerdanyola del Vallès, Spain) for the sample A only. The data were collected in a 2° to 73° 2θ range at a wavelength of $\lambda = 0.8261 \text{ \AA}$. The sample A was enclosed in a 0.5 mm-diameter sealed glass capillary. The laboratory XRD characterization of the samples B and C was performed at room temperature on a PANalytical X'Pert Pro with a X'Celerator detector and equipped with $K_{\alpha_{1,2}}$ radiations. The radiations were generated at 35 kV and 30 mA ($\lambda(K_{\alpha_1}) = 1.789 \text{ \AA}$ and $\lambda(K_{\alpha_2}) = 1.793 \text{ \AA}$). The measurements were performed between 10° and 80° . The profile refinements and structure refinements using the Rietveld method were realized with the software FullProf developed by J. Rodriguez-Carvajal³⁷.

1D Solid-State NMR: The samples A, B and C were introduced in 2.5 mm zirconia rotors inside a glovebox. ^7Li MAS NMR spectra were acquired using a Bruker Avance (7.05 T magnet) spectrometer at 116.6 MHz and a Bruker Avance III spectrometer with a 2.35 T magnet at 38.9 MHz using a standard Bruker 2.5 MAS probe at a 30 kHz spinning frequency. A Hahn echo sequence was applied with a 90° pulse of 1.1 μs and 2 μs respectively on the 7.05 T and 2.35 T magnets. Recycle delay of 5 s was long enough to avoid T_1 saturation effects and all the shifts are referred to a 1M LiCl (aq) solution. ^{23}Na MAS NMR was performed on a Bruker Avance spectrometer at 79.4 MHz (7.05 T magnet) and 132.3 MHz (11.75 T magnet). As ^{23}Na is a strong quadrupolar nucleus with $I = 3/2$, a short pulse length of 1 μs corresponding to a $\pi/8$ pulse determined using an aqueous 1 M NaCl solution was employed. In these conditions, the main signal observed is due to the $-1/2 \rightarrow +1/2$ central transition. The spectral width was set to 1 MHz, and the recycle time $D_0 = 0.5 \text{ s}$, is long enough to avoid T_1 saturation effects. The baseline distortions

resulting from the spectrometer dead time (8 μ s) were computationally removed using a polynomial baseline correction routine with the software DMFit³⁸. DMFit was used for all the fitting processes.

⁷Li and ²³Na variable temperature 1D NMR experiments were carried out on a Bruker 300 Avance spectrometer in the 265 K - 450 K range using a Bruker 4 mm WVT MAS probe. A spinning frequency of 13 kHz was used. The temperature calibration was realized using lead nitrate^{39,40}. Along the rotor a temperature gradient up to 5K can be observed also 80% of the sample was observed at the desired temperature \pm 1K.

Selective inversion ⁷Li MAS NMR: Only the sample B was analyzed with this technique. For the selective inversion ⁷Li MAS NMR experiments, a probe for 1.3 mm-diameter zirconia rotors (spinning frequency = 65 kHz) was used on a Bruker 300 Avance spectrometer with a Larmor frequency of 116.6 MHz. 90° pulse length was set at 3 μ s and recycle time at 5 s. For all acquisitions, mixing times (τ_{mix}) were set from 0.05 ms to 6 s. Selective inversion consists of a succession of two pulses separated by a mixing time, 180°- τ_{mix} -90°. The 180° pulse is a soft power Gaussian shaped pulse (40 dB) with a length of 900 μ s in order to probe one selected site. The phase sensitive detection in T_1 was achieved through the use of States-TPPI. 1 M LiCl was used as standard (0 ppm).

Magnetic measurements: The molar magnetic susceptibility versus temperature was extracted from magnetization measurements as a function of the temperature from 7 K to 300 K using a constant field of 1 T with Super Quantum Interference Device (SQUID) magnetometer MPMS5. Only the sample A was analyzed and was cooled without any application of magnetic field (Zero Field Cooling).

Conductivity measurements: Transport properties were measured on cold-pressed pellets, the compactness of which was close to 70%. Electrical DC conductivity measurements were performed with the aligned four-probe method in the 4.2-300 K range using a home-made equipment.

3. Results and Discussion

Despite reproducing the synthesis many times with slightly different alkaline initial compositions, a real pure OP4 phase could not be obtained since, as discussed below, traces of impurity phases were always observed by XRD. Among all the prepared samples, we selected for the discussion in this paper, three of them, representative of all the resulting powders.

XRD characterization of the samples

Figure 2 shows the XRD patterns of the three samples as a function of the d spacing in Å, as all the XRD patterns were not recorded at the same wavelength. The insert represents the most intense diffraction line, (004) at $d = 5.1$ Å. The three samples exhibit, in addition to the diffraction lines expected for the OP4 phase, extra peaks indicating the presence of one or two phases as impurities : O3-LiCoO₂ is present as traces in Sample A as seen on the zoom of Figure 2 by the presence of its (003) diffraction line at 4.7 Å ; P2-Na_{~0.7}CoO₂ and OPP9-(Li/Na/Na)CoO₂ phases¹⁸, are present as traces in Sample B as seen on the zoom by the presence of the (002) peak of P2 at 5.4 Å and (009) peak of OPP9 at 5.2 Å; OPP9 is only present as traces in Sample C (**Figure 2**). All these structures are represented on **Figure S3**. Our quenching procedure was fast enough to avoid the OP4 phase decomposition in O3-LiCoO₂ and P2-Na_{~0.7}CoO₂ observed previously¹⁸, since these two phases are not simultaneously observed. The XRD patterns of all the phases were refined using the Le Bail method to extract the cell parameters as summarized in **Table 2**. The refined lattice

parameters of the OP4 phase, $a_{\text{hex.}} \sim 2.824(2) \text{ \AA}$ and $c_{\text{hex.}} \sim 20.28(1) \text{ \AA}$, are in good agreement with the values ranges reported in the literature (**Figure S1**). The refined cell parameters of the O3-LiCoO₂, P2-Na_{~0.7}CoO₂ and OPP9-(Li/Na/Na)CoO₂ impurities phases are also in agreement with the literature^{10,14,18}. The structural Rietveld refinement of the SXRD data for sample A will be discussed only at the end of the paper. Indeed, the NMR characterization, discussed below, will provide new structural information.

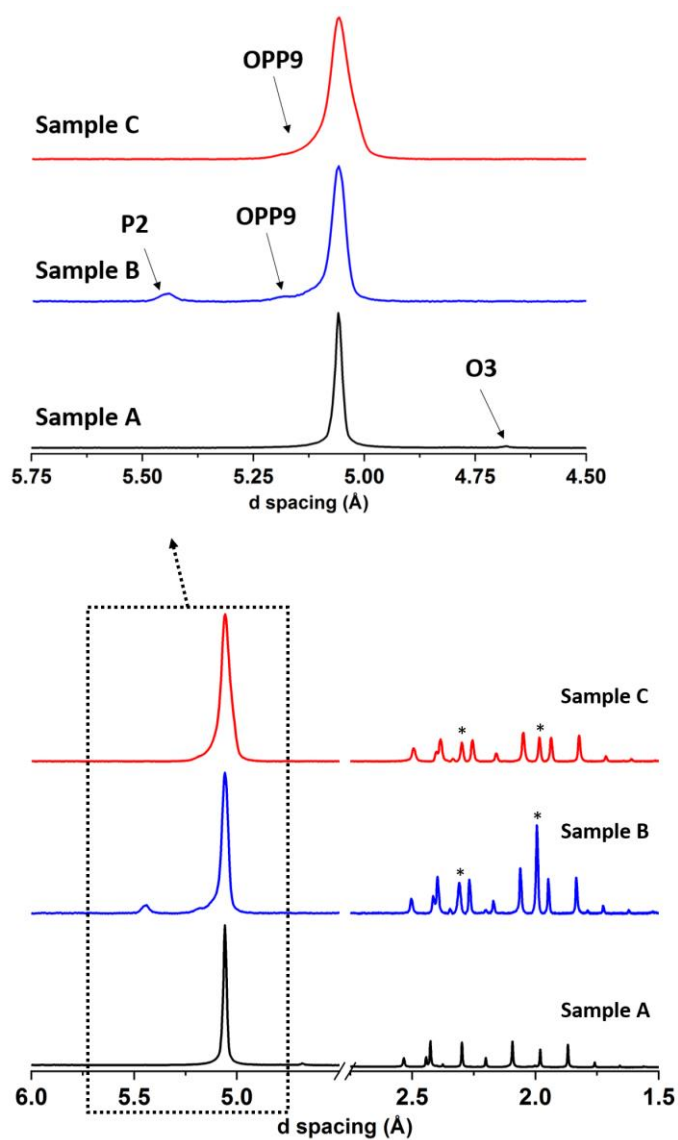


Figure 2: Experimental XRD patterns of the samples A, B and C plotted as a function of the d spacing. Insert: Zoom in the 5.75 Å- 4.50 Å region in order to focus on the impurities peaks. * are the Al peaks due to the sample holder used for the XRD acquisitions.

		Sample A	Sample B	Sample C
OP4 (P6₃/mmc)	a_{hex}	2.826(1) Å	2.826(3) Å	2.822(1) Å
	c_{hex}	20.29(3) Å	20.28(3) Å	20.28(2) Å
O3 (R3c)	a_{hex}	2.81(2) Å	-	-
	c_{hex}	14.08(8) Å		
P2 (P6₃/mmc)	a_{hex}		2.838(3) Å	
	c_{hex}		10.92(1) Å	
OPP9 (R3m)	a_{hex}		2.835(3) Å	2.837(2) Å
	c_{hex}		46.7(2) Å	46.1(2) Å

Table 2: Refined lattice parameters of the different phases reported in the samples A, B and C

Local structure, electronic structure and dynamics from ⁷Li MAS NMR

The 1D ^7Li MAS NMR spectra of the three samples are shown in **Figure 3**. They all exhibit 5 signals located after fitting at 32, 18, 0, -84 and -203 ppm and respectively labelled 1 to 5 on **Figure 3a**. Such wide peak shifts distribution and shifts values are characteristics of the presence of several Li paramagnetic environments as expected from the $\text{Li}_{0.42}\text{Na}_{0.38}\text{CoO}_2$ stoichiometry, with formally 0.2 LS-Co^{4+} (t_{2g}^5) paramagnetic ions. The local environment of the Li^+ ions in the lattice is shown in **Figure 1b**: Li is surrounded by 6 Co ions through 180° Co-O-Li interaction and 6 Co ions through 90° Co-O-Li interaction, similarly to the Li environment in stoichiometric $\text{O}_3\text{-LiCoO}_2$. In the later compound Li is only surrounded by LS-Co^{3+} with the diamagnetic $t_{2g}^6e_g^0$ electronic configuration. A single signal ~ 0 ppm is therefore observed by ^7Li MAS NMR^{10,41-44}. As the OP4 phase exhibits several ^7Li signals, this indicates that Co ions with different local electronic structures are present around Li, probably due to the arrangement of the Na^+ /vacancy in the next cationic layer. Only signal 3 can be assigned to Li^+ ions in diamagnetic LS-Co^{3+} environment. The spectra were also recorded at different magnetic field strengths (2.35 T and 7.05 T) to confirm the number of peaks and the origin of the lineshape (**Figure 3b**). While higher magnetic fields are useful for reducing the broadening due to both, nuclear-nuclear dipolar interactions and quadrupolar interactions, the associated increase in broadening due to stronger electron-nuclear dipolar interactions results in rather similar final line widths and resolution. However, since the same 30 kHz spinning frequency was used in both experiments, the spectra recorded at 2.35 T exhibit less spinning side bands and therefore more intensity in the isotropic positions. The advantage is clearly seen for the negatively shifted signal that exhibits a wider spinning side bands distribution than the others. Moreover, at low 2.35 T field, a weak signal labeled “5” can be clearly observed at -203 ppm and was located under a spinning side band using the 7.05 T magnet. After fitting the spectra (**Figure 3c**), the resulting signal intensities (including the spinning side bands) have been extracted and summarized in **Table 3**. Signal 5 was not considered because of its very

low intensity. The intensity values obtained for the signal 2 are similar for all the samples and are therefore not affected by the nature of the impurities in the samples. Contrary to Signal 2, Signal 3's intensity is slightly more intense for Sample A in agreement with the presence of O3-LiCoO₂ as impurity.

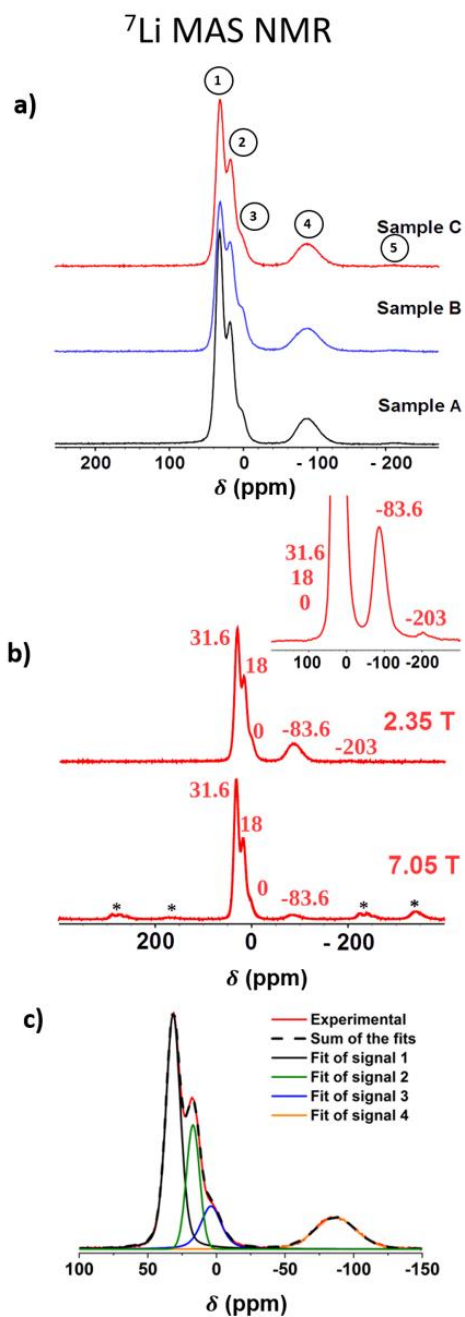


Figure 3: (a) Experimental ^7Li MAS NMR spectra for the samples A, B and C (2.35 T magnet, $\nu_R = 30$ kHz, Hahn echo sequence). (b) Comparison of the ^7Li MAS NMR spectra recorded for the sample C at two different magnetic fields (2.35 and 7.05 T) using the same spinning frequency (30 kHz). (c) Fits of the signals 1, 2, 3 and 4 compared to the experimental spectra for Sample C (with no Li-phase as impurity). * represents the spinning side bands.

	Signal 1 (32 ppm)	Signal 2 (18 ppm)	Signal 3 (0 ppm)	Signal 4 (-84 ppm)
Sample C	47%	19%	12%	22%
Sample B	52%	18%	11%	19%
Sample A	41%	19%	18%	22%

Table 3: Repartition of the fitted areas of each ^7Li signal for the three studied samples. The signal 5 was neglected here because of its low intensity.

Variable temperature MAS NMR experiments (**Figure 4**) using a 13 kHz spinning frequency in a $265\text{ K} \leq T \leq 450\text{ K}$ temperature range were performed initially in order to investigate the possibility of Li site exchange, but actually provided really interesting information about the nature of the NMR shifts observed for the OP4 phase. No exchange phenomenon was observed in this $265\text{ K} \leq T \leq 450\text{ K}$ temperature range and the spectrum at 300 K was fully recovered after the experiment. Note that at 450 K, one can also distinguish a new component labelled 3'. The variation of the signals position reveals the complexity of the origin of the shifts. The position of Fermi contact shifted signals, in paramagnetic compounds, are expected to follow the same trend as does the magnetic susceptibility (equation 1), *i.e.*, varies as $1/(T-\theta)$ and tends to diamagnetic chemical range (near 0 ppm for Li) as T tends to $+\infty$. For the OP4 phase, this is not the case; especially the position of the signal 2 remains almost temperature independent, also confirmed by higher resolution

experiments performed at 30 kHz (**Figure S4**). The evolution of the shifts position versus temperature is plotted in **Figure 5a**.

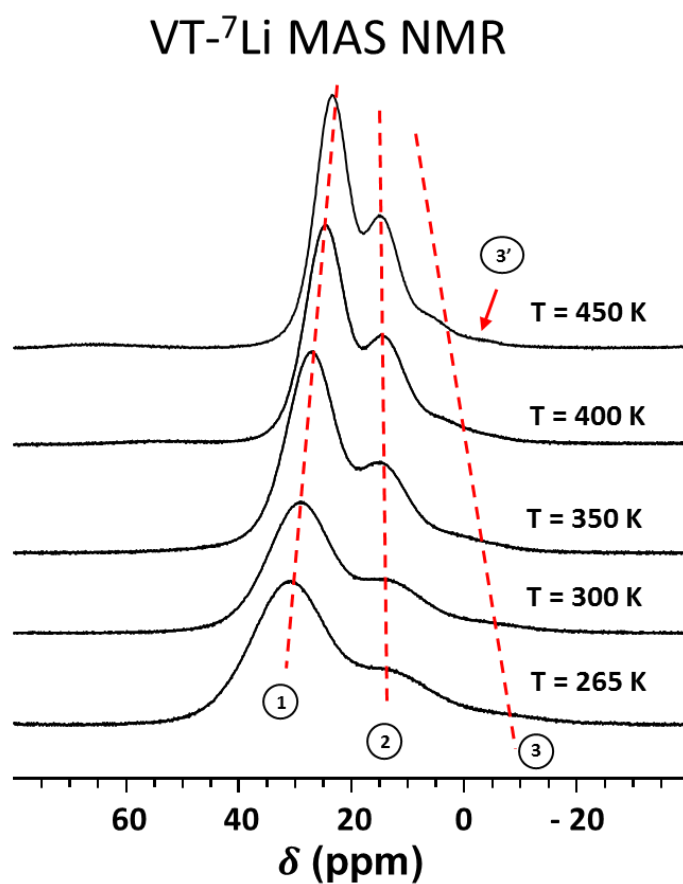


Figure 4: Experimental ^7Li MAS NMR spectra performed on the sample B on a 7.05 T magnet at different temperatures in the 265 K – 450 K. The NMR sequence was a Hahn echo sequence and the spinning frequency was 13 kHz.

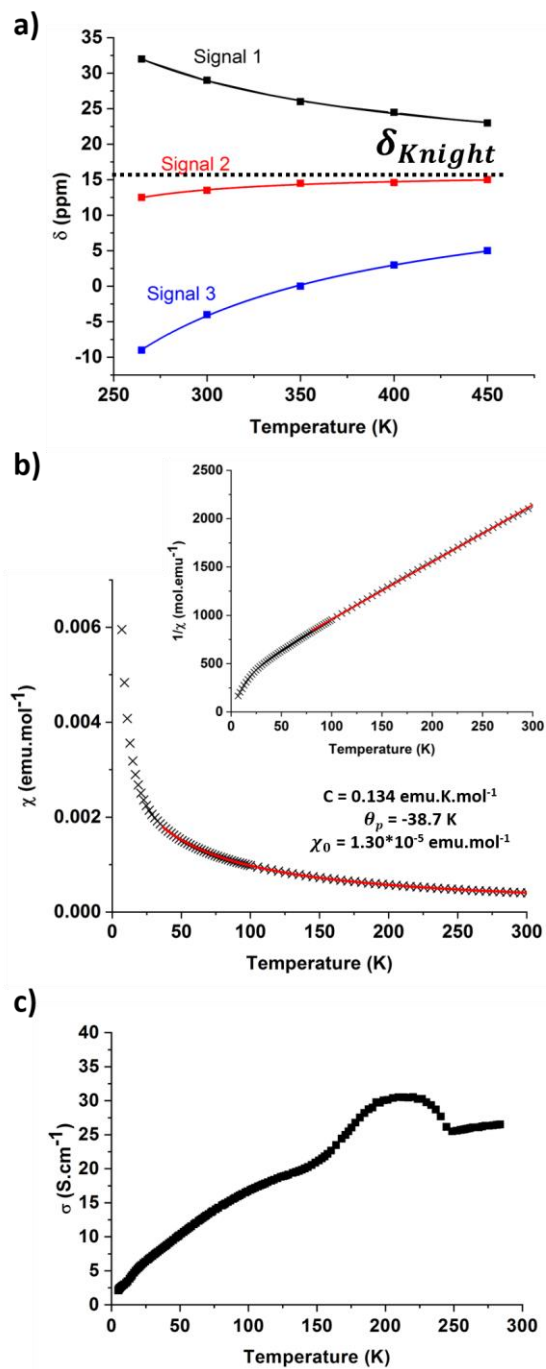


Figure 5: (a) Fitted lines of NMR shifts evolution of the signals 1, 2 and 3 as a function of the temperature. (b) Magnetic susceptibility and inverse magnetic susceptibility of the sample A (insert) as a function of the temperature (6 K to 300 K). (c) Electrical conductivity of the sample A as a function of the temperature (6K to 300 K).

In order to better understand the temperature evolution of the signals, the magnetic susceptibility (**Figure 5b**) and the electrical conductivity (**Figure 5c**) of the OP4 phase were also studied. The fit of the experimental magnetic measurements was realized taking into account a paramagnetic contribution, following a Curie-Weiss law and a temperature independent term χ_0 (thus $\chi(T) = \frac{C}{T-\theta_p} + \chi_0$). The fitted values are $C = 0.134 \text{ emu.K.mol}^{-1}$, $\theta_p = -38.7 \text{ K}$ and $\chi_0 = 1.30 \cdot 10^{-5} \text{ emu.mol}^{-1}$. The C value is relatively high compared to theoretical one ($C_{th} = 0.05 \text{ emu.K.mol}^{-1}$) by considering the $\text{Li}_{0.42}\text{Na}_{0.38}\text{CoO}_2$ formula with 0.2 LS-Co^{IV} and 0.8 LS-Co^{III}. This difference indicates that the material doesn't completely follow a Curie-Weiss law and a part of the susceptibility can be due to delocalized electrons. The evolution of the electrical conductivity (**Figure 5c**) denotes a semi-conductor behavior probably due to inter particles boundaries resistivity. Ren *et al.*¹⁵ reported similar data as well as Seebeck coefficient measurements that showed that the OP4 phase should exhibit a metallic conductivity in the (a, b) plane relatively similar to the P2-Na_xCoO₂^{45,46} and O3-Li_xCoO₂⁴⁴ phases. Our VT-MAS NMR results are further confirming the dual character of the OP4 phase that exhibits delocalized electrons and localized ones. Indeed, the temperature evolution of the ⁷Li MAS NMR shifts can be interpreted considering that the shifts result from two interactions: the Fermi contact interaction (for localized electrons), that is temperature dependent, and the Knight shift contribution (for delocalized electrons) that is temperature independent. The total shift for a *i* nucleus can be expressed by:

$$\delta_{tot}^i(T) = \delta_{Fermi}^i(T) + \delta_{Knight}^i \quad \text{eq. (3)}$$

By fitting the evolution of the signals position versus T (**Figure 5a**), the ⁷Li MAS NMR shifts tends toward a rather similar Knight shift contribution for all the signals to $\sim 16 \text{ ppm}$ for $T \rightarrow +\infty$ (**Table 4**). This position is clearly out of range of the chemical shift for ⁷Li in diamagnetic environment

and can be, indeed, attributed to a Knight shift component. The Fermi contact coupling constant incorporated in a constant labelled B for this paper ($B = \frac{c}{3SN_A} \rho^i(0)$), is found to be either positive or negative depending on the signals (**Figure 5a**). A positive contribution is expected for a 90° LS- Co^{IV} -O-Li interaction (delocalization mechanism) while a negative shift is expected for a 180° LS- Co^{IV} -O-Li interaction similarly to the case of $\text{Li}(\text{Co}^{\text{III}}_{1-y}\text{Cr}^{\text{III}}_y)\text{O}_2$ phases^{30,48}. Note that no comparison with the shift obtained for the Li_xCoO_2 samples was possible, since in this system, it was concluded that the formation of localized Co^{4+} ions at the beginning of the deintercalation leads to a loss of observation of adjacent Li^+ and then an insulator to metallic transition occurs and leads to the observation of a single Knight shift located around 60 ppm⁴⁴.

	Signal 1 (32 ppm)	Signal 2 (18 ppm)	Signal 3 (0 ppm)
B (ppm.K)	2400 ± 500	-270 ± 150	-3700 ± 500
θ_p (K)	115 ± 20	200 ± 30	120 ± 15
δ_{Knight} (ppm)	16 ± 1	16 ± 1	16 ± 1

Table 4: Calculated values for B, θ and δ_{Knight} after the fitting of the curves showed on Figure 5a.

Density Functional Theory (DFT) calculations can be used to assign the Fermi contact signals and better understand the local electronic structure^{27,29-31}. Unfortunately, neither Generalized Gradient Approximation (GGA) nor GGA+U allow a correct description of the electronic structure of such

layered cobalt oxides. In GGA, the inherent self-interaction error has a detrimental effect on localized transition-metal d orbitals. Although, the addition of a Hubbard U correction can produce theoretical average voltages or Fermi contact shifts in better agreement with experiments⁴⁸, this method is not used in this study because it has been shown to yield some unphysical results for layered cobalt oxide systems: phase stability inversion between O1 and O3 in CoO₂ and incorrect phase diagram for the P2-Na_xCoO₂ system⁴⁹. On the contrary, GGA has been successfully used to describe the phase diagram of the Li_xCoO₂ system⁵⁰ and the metallic conduction⁴⁴. Even if the electronic structure could not be properly described using DFT, our results considering a Li_{0.5}Na_{1/3}CoO₂ [Li₂₄Na₁₆Co₄₈O₉₆ supercell] model compound with a full Li layer as in O3-LiCoO₂ and the Na⁺/vacancy ordering reported by Platova *et al.*⁵¹ for P2-Na_{2/3}CoO₂, are given in **Figure S5.1**. Our calculations indicate that the t_{2g} Co orbitals degeneracy is lifted because of the CoO₆ distortion along the c axis leading to a_{1g} and e_g' orbitals⁷. The 3D spin density map shows that the a_{1g} orbital is mainly carrying the electron spins (**Figure S5.3c**). Nevertheless, the e_g' orbitals involving the t_{2g} ones that overlap through the middle of the CoO₆ common edge of the octahedra should be responsible for the delocalized behavior in the (a,b) plane while electrons in the a_{1g} oriented along c should be mostly responsible for the localized character. The schematic band structures for TM ion in O_h symmetry and D_{3d} symmetry when the octahedra are distorted along the c axis, are shown on **Figure 6** and highlights the presence of the localized electrons and the delocalized electrons. The Fermi contact shift calculations indicate that considering a specific Na ordering in the sodium layer, tends to partially localize the charges on the Co ions and leads to slightly different Li electronic environments and several Li calculated shifts. Even if a complete signal assignment could not be proposed here, we demonstrated that NMR can be successfully used to investigate the local electronic structure of materials, in particular, here, it provides information about the complex electronic structure of layered cobaltates with some localized and delocalized

electrons and the presence of Co ions with different local electronic structures around Li ions, probably due to the arrangement of the Na^+ ions in the next cationic layer.

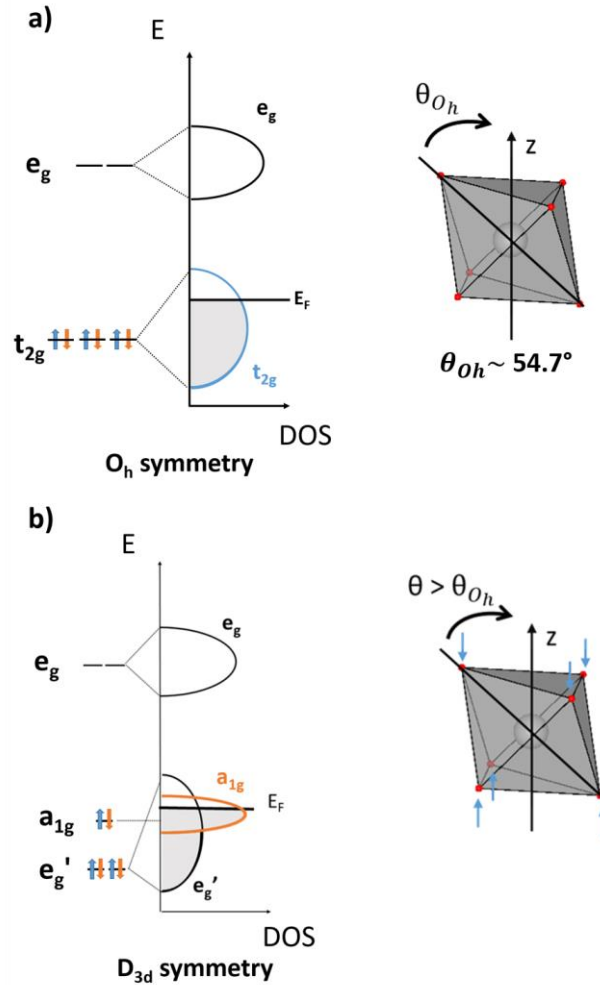


Figure 6: Schematic representation of the band structure of the Co ions in layered alkali cobaltates (a) without and (b) with considering the octahedra distortion perpendicular to the CoO_2 layers. The inserts correspond to the CoO_6 octahedron in each case. The θ angle represent the angle between the z axis parallel to the c_{hex} parameter and a Co-O bond direction. For a regular octahedral $\theta = 54.7^\circ$, whereas $\theta \sim 61.2^\circ$ in the OP4 phase.

According to our VT- MAS NMR experiments (**Figure 4 and S4**), no evidence for Li^+ mobility was observed up to 450 K. However, by using selective inversion experiments, one can investigate possible lithium ions motion at different timescales³⁶. This sequence introduces a mixing time,

which allows a magnetization exchange between the different Li sites. The advantage of this technique is the fact that many data points can be collected compared to other 2D NMR techniques allowing modeling efficiently the relaxation of the magnetization back to equilibrium. Selective inversion is also a good technique in order to calculate the rate constants of the different Li⁺ sites if ionic mobility is observed. By processing at different temperatures, the activation energies can also be determined. This technique proposes to initially invert selectively one Li signal using the Gaussian shaped soft pulse. The mixing times allow then the magnetization to return to equilibrium. During the different mixing times (and T_1 relaxation), chemical exchanges between the inverted and the none-inverted Li signals are possible if Li⁺ ions are able to hop from one site to the other. The consequence on the NMR spectra is a buildup of magnetization due to the potential chemical exchanges and the T_1 relaxation for the inverted/probed signal. For the non-inverted signals, an attenuation of their intensities characterizes an ionic mobility in the structure due to the chemical exchange with the inverted signal. **Figure 7** shows the selective inversion spectra with the different mixing times recorded on the sample B at 340 K. Only the inversions on the signal 1 are shown in this paper. The signal 2 shows a slight modification of its intensity with the mixing time evolution. That could be due to the weak separation between the probed signals 1 and the signal 2, in fact, it is probably slightly affected by the soft pulse applied on the signal 1. By probing the other signals, no dynamics involving hopping rates higher than the frequency gap between signals (typically ~1500 Hz) is observed (**Figure S6**). This result is the same whatever the temperature in the RT – 330 K range. Thus, no Li⁺ ions mobility can be highlighted by dynamic MAS NMR in the timescale that was probed. No dynamics is observed faster than 6 s involving full or almost full Li layers. The occupancy of the Li layers will be discussed with Rietveld refinement of the structure of the sample A using the SXRD data.

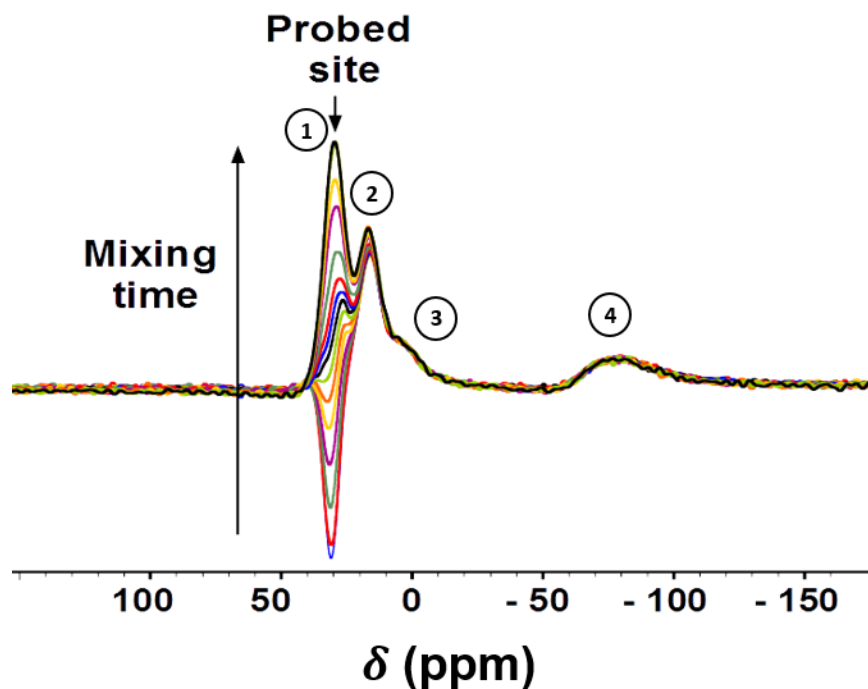


Figure 7: Experimental ${}^7\text{Li}$ MAS NMR spectra of the sample B with the selective Inversion (SI) technique performed at 340 K with mixing times from 0.05 ms to 6 s. The signal 1 was selectively inverted on this Figure. The acquisitions were realized on a 7.05 T magnet with a spinning frequency of 65 kHz.

Local structure, electronic structure and dynamics from ${}^{23}\text{Na}$ NMR

Figure 8a shows the ${}^{23}\text{Na}$ MAS NMR spectra recorded for the three $(\text{Li},\text{Na})\text{CoO}_2$ compounds under a 11.75 T magnetic field. The local prismatic environments of Na in the OP4 phase are shown in **Figure 1b**. Considering their large values, the ${}^{23}\text{Na}$ NMR shifts are mainly due to the hyperfine interactions between Co unpaired electrons and Na nuclei spin⁵³. We recorded the spectra under

different magnetic field strengths (7.05 T and 11.75 T) (**Figure 8b**): the 11.75 T magnetic field strongly decreases the 2nd order quadrupolar broadening, but does not allow to suppress it. It, however, allows getting a rather good resolution and to distinguish several contributions for Na in the structure. In sample A, which does not exhibit any impurities containing Na ions (no P2 nor OPP9 phases) two signals are observed around 300 and 200 ppm. Both signals could be further fitted using a 2nd quadrupolar lineshape (**Figure 8c** and **Table 5**). The main signal (signal 2 in **Figure 8**) corresponds to an average signal for the Na⁺ ions in the Na_e and Na_f sites in the Na layers due to high ionic mobility of Na⁺ ions at the NMR time scale as already observed for P2-Na_xCoO₂⁵², P2-Na_{2/3}Co_{2/3}Mn_{1/3}O₂⁵³, P2-Na_xFe_{1/2}Mn_{1/2}O₂⁵⁴ and P2-Na_x[Li_yNi_zMn_{1-y-z}]O₂²⁸. The high Na⁺ mobility in P2-type of structure was also evidence in P2-Na_{1/2}VO₂ above 325K, as the V-V trimers are suppressed⁵⁵. **In Figure 8**, the second less intense signal observed for the OP4 phase (signal 1), then denotes the presence of Na⁺ ions that would not take part to this exchange, therefore most probably not in the interslab space. We argue that this signal might correspond to the presence of some Na⁺ ions in the Li layers, therefore in octahedral site (**Figure 1**). The larger shift observed for this signal could result from the shorter Co-O-Na distances that would induce stronger hyperfine interaction. This new structural hypothesis will be taken into account for the Rietveld refinement of the synchrotron XRD pattern below. Note that samples B and C exhibit the same two signals (signal 1 and signal 2 in **Figure 8**), but also an additional one located around 360-380 ppm, whose position corresponds to Na in Na_{~0.7}CoO₂⁵² and can be assigned to Na⁺ in environments similar to the P2 phase (P2 and OPP9 impurities).

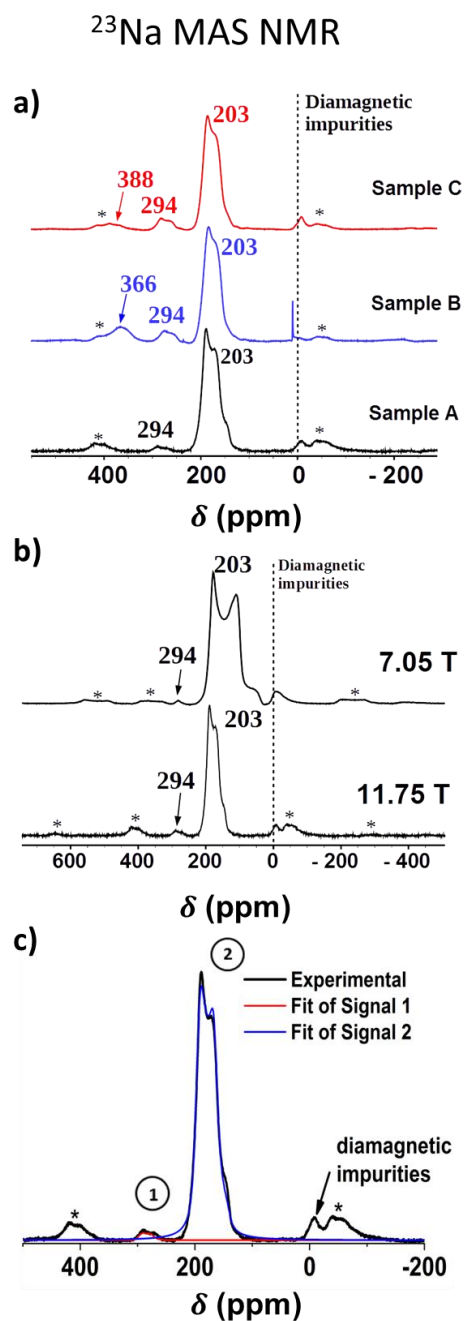


Figure 8: (a) Experimental ^{23}Na MAS NMR spectrum of the three studied samples with performed on a 11.75 T magnet at a spinning frequency of 30 kHz. (b) Comparison of the ^{23}Na MAS NMR spectra recorded of the sample A for two different magnetic fields (7.05 T and 11.75 T). (c) Fits of the signals 1 and 2 recorded by NMR on sample A compared to the experimental spectra. 2nd order quadrupolar lineshapes were used to fit the spectrum and the corresponding parameters are provided in Table 5. * Represent the spinning side bands.

		δ_{iso} (ppm)	Repartition of the areas (%)	C_Q (MHz)	η	lb (ppm)
Sample C	Signal 1	294	8	3.92	0.35	8.23
	Signal 2	203	92	4.14	0.33	8.32
Sample B	Signal 1	294	7	3.57	0.37	10.3
	Signal 2	203	93	4.09	0.38	9.46
Sample A	Signal 1	294	2	3.58	0.39	6.50
	Signal 2	203	98	4.19	0.25	11

Table 5: Repartition of the areas of the two signals highlighted on the ^{23}Na MAS NMR spectra for Na^+ ions for the three studied samples and NMR parameters for each signal calculated with the DMFit software³⁸. The signals around 370 ppm on the samples B and C spectra are not considered because they are due to Na impurities. For each parameter, the last number falls into the error bar. δ_{iso} (ppm) = the isotropic position ; C_Q (MHz) = the quadrupolar coupling constant; η = the asymmetry parameter of the quadrupolar interaction tensor and lb (ppm) = broadening factor.

^{23}Na MAS NMR variable temperature experiments were also performed with a spinning frequency of 13 kHz between 265 and 450 K (**Figure 9a**). Note that using a 13 kHz spinning frequency and a 7.05 T magnetic field, the resolution was not sufficient to follow the change of the signal 1. In **Figure 9b and S7**, the evolution versus T of the fitted parameters using a 2nd order quadrupolar lineshape are provided for signal 2. As temperature increases, a decrease of the shift values is observed as expected for paramagnetic shifts. However, in the case of ^{23}Na MAS NMR, contrary to ^7Li , one cannot neglect the quadrupolar shift contribution to the total shift in addition to the Fermi contact and the Knight shifts. The analysis of the isotropic shift position versus the temperature is therefore more complex than for ^7Li . The temperature increase, also results in a sharpening of the signal that exhibits at 450 K a well-defined 2nd order line shape. This signal modification can be interpreted by i) an increase of the Na^+ ions motion in the interslab spaces that

is not fully achieved at room temperature compared to the NMR timescale and ii) a decrease of the dipolar part of the nuclear–electron spin coupling as also observed for the P2-Na_xCoO₂⁵². According to our previous VT-²³Na NMR study of P2 and P3-Na_xCoO₂ polymorphs, the increase of Na⁺ ions mobility is rather due to an increase of the hopping rate between Na sites in the interslab space than to an increase of movement/vibration of the Na⁺ ion around its average position⁵². It also appears that the quadrupolar interaction increases as the temperature increases, that may be linked with the change of the interslab distances modification upon heating that was not studied here.

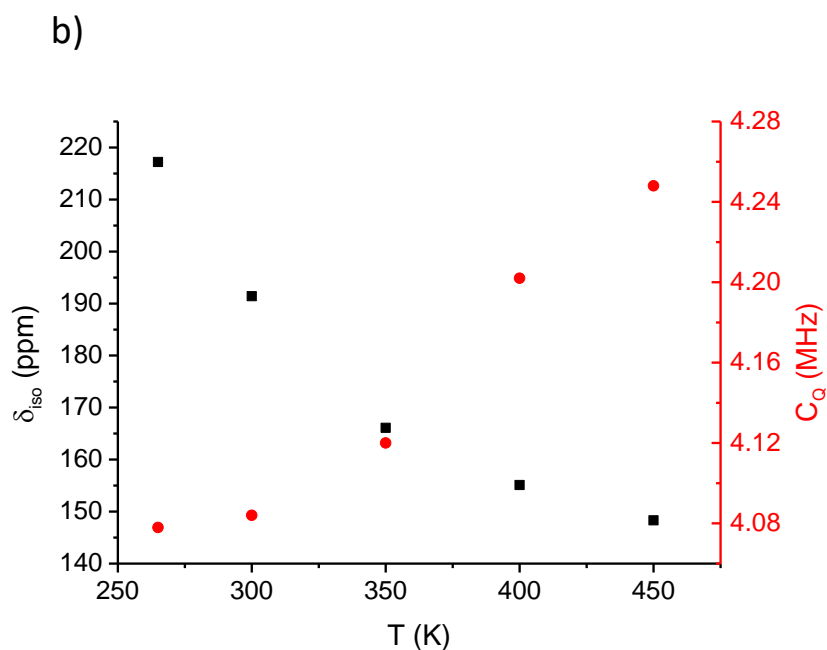
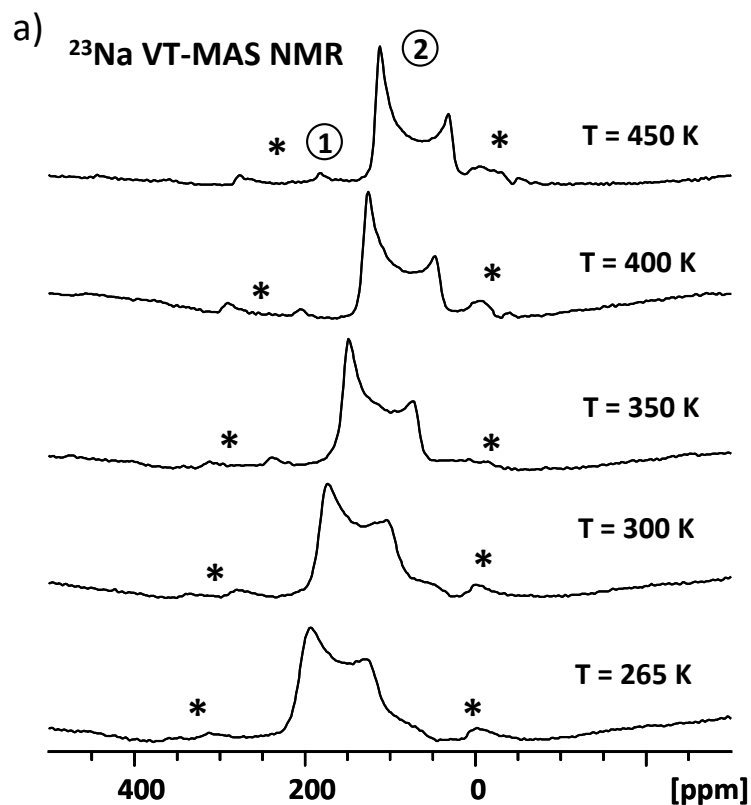


Figure 9: a) VT- ^{23}Na MAS NMR recorded on a 7.05 T magnet at a spinning frequency of 13 kHz in the 265 K < T < 450K range. * are the spinning side bands. Note that a diamagnetic impurity is also seen around 0 ppm. b) Evolution of the some of the fitted parameters using a 2nd order quadrupolar lineshape. δ_{iso} = isotropic position (ppm); C_Q = quadrupolar coupling (MHz). All fitted values are provided in Figure S7.

Average structure from synchrotron XRD Rietveld refinement

Our ^{23}Na MAS NMR study indicates that some Na^+ ions might be located in the Li layers in the OP4 phase. Such a possibility was therefore further considered in the structural model refined by the Rietveld method using the SXRD data. A good agreement between the calculated pattern and the experimental one can be thus achieved (**Figure 10**). The resulting fitted parameters are given in **Table 6**. Note that the refinement allows determining that the sample A is composed of 3 % of LiCoO_2 and 97 % of the OP4 phase. Considering the low amount of the O3 phase, inductively coupled plasma atomic emission spectrometry (ICP-AES) measurements led in that case a relative good agreement between the target and experimental Li/Co and Na/Co ratios (0.42(1) and 0.37(1) respectively) in good agreement with our previous study¹⁸. The slight peak asymmetry (**insert on Figure 10**) suggests the presence of a low amount of stacking faults in the structure as suggested by Berthelot *et al.*¹⁸. For the refinement, we fixed the Co, O and Li stoichiometry respectively to 1, 2 and 0.42. Therefore, only the occupancies of the Na sites were refined considering the possibility of having Na^+ ions in the Li site. As a result, we found 0.05(1) Na^+ in the O-type interslabs of the OP4 phase leading to a global occupation of ~ 95 % of the Li layers. The P-type interslabs exhibit more vacancies, since they are filled at 64(1) % by Na^+ ions. The resulting chemical formula is therefore $\text{Li}_{0.42}\text{Na}_{0.37}\text{CoO}_2$, in good agreement with the target composition and can be more specifically written as $\text{OP4-}[\text{Li}_{0.42}\text{Na}_{0.05}]\text{Na}_{0.32}\text{CoO}_2$ from our ^{23}Na and SXRD data. The resulting refined Li-O, Na-O and Co-O distances are shown in **Figure 11**.

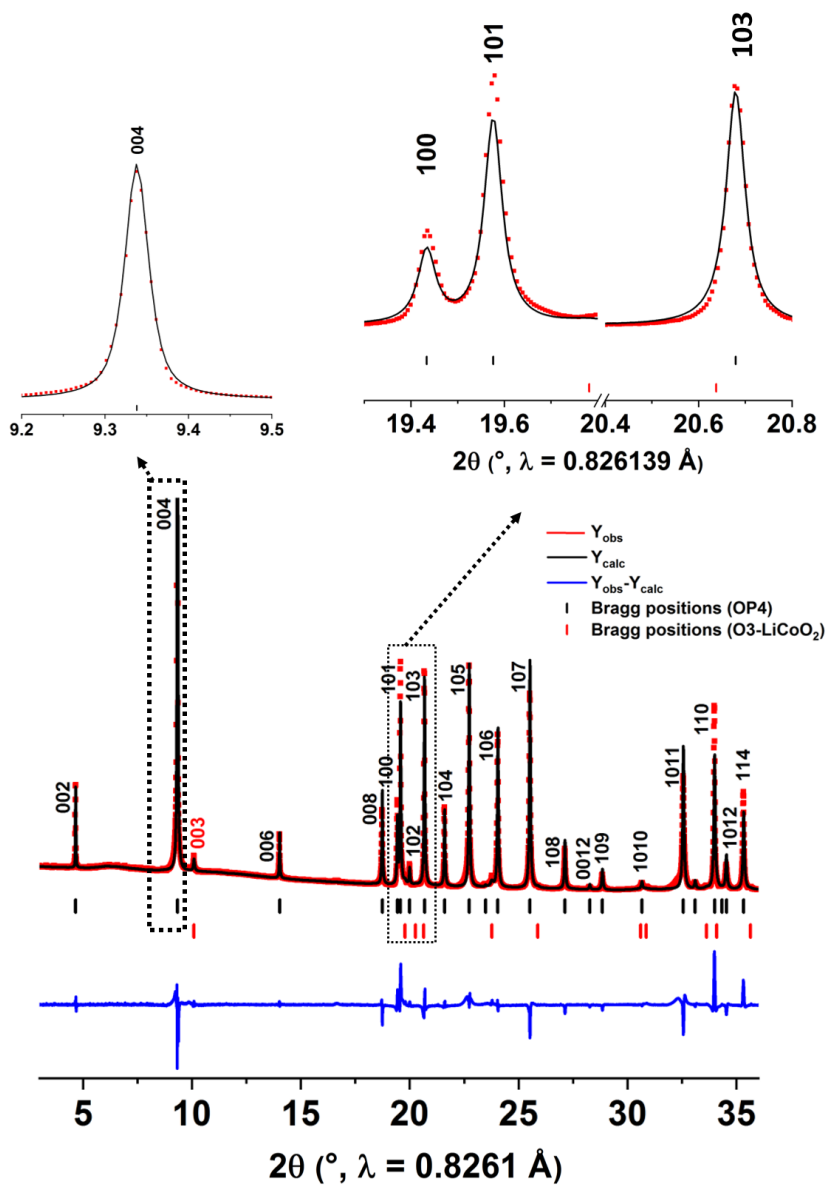


Figure 10: Synchrotron XRD pattern as a function of the 2θ position of the sample A with $\lambda = 0.8261 \text{ \AA}$. Red bars and black bars correspond, respectively, to the Bragg positions of O3-LiCoO_2 and OP4-(Li/Na)CoO_2 . Red points correspond to experimental XRD pattern while black line is the calculated one obtained by Rietveld refinement. The blue line is the difference between experimental and calculated lines.

Space group : $P6_3/mmc$						
$a_{\text{hex.}} = 2.826(1) \text{ \AA}$			$c_{\text{hex.}} = 20.298(3) \text{ \AA}$			
Atom	Site	x	y	z	B (\AA^2)	Occ.
Co	4f	2/3	1/3	0.3836(2)	0.64(1)	1
Na _f	2d	2/3	1/3	0.25	1.2	0.21(1)
Na _e	2c	1/3	2/3	0.25	1.2	0.43(1)
Li	2a	0	0	0.5	0.9	0.84
Na (Li layer)	2a	0	0	0.5	0.9	0.10(1)
O _{Na}	4e	0	0	0.3363(7)	0.79(1)	1
O _{Li}	4f	1/3	2/3	0.4248(7)	0.42(1)	1

Rp = 14.1 %	U = 0.0109(5)
Rwp = 15 %	V = -0.0066(5)
	W = 0.0005(5)
	X = 0.10(1)
	Y = 0.0091(2)

Table 6: Calculated parameters, atomic positions and occupancies obtained for the refined SXR D data performed on the sample A (SXR D pattern on Figure 10) with the $P6_3/mmc$ space group. O(Na) represent the O ions between Na and Co layers while O(Li) are the O ions between Li and Co layers.

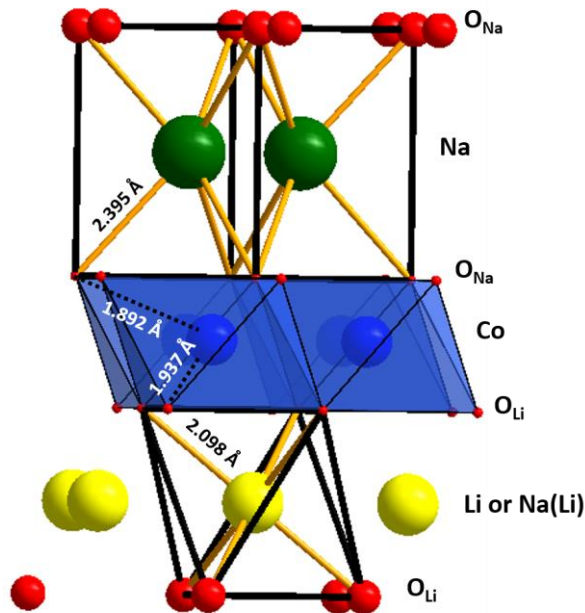


Figure 11: Bonds distances, in Å, calculated after Rietveld refinement of the OP4 phase.

Conclusion

The reinvestigation of the original OP4- $\text{Li}_x\text{Na}_y\text{CoO}_2$ phase, by solid state NMR and synchrotron XRD led to a better understanding of the material structure, electronic structure and dynamics. ^7Li MAS NMR shows that the NMR shifts result from two contributions: the Fermi contact and the Knight shifts due to the presence of both localized and delocalized electrons. This is good agreement with the complex electronic structure expected for layered cobalates, as the t_{2g} Co orbital undergo a lift of degeneracy due to CoO_6 octahedra distortion perpendicular to the layer (D_{3d} symmetry). ^7Li MAS NMR clearly shows several Li environments indicating that, moreover, Co ions with different local electronic structures are formed, probably due to the arrangement of the Na^+ ions in the next cationic layer. Unfortunately, those materials are really difficult to model properly using DFT calculations and no complete signal assignment could be proposed. ^{23}Na MAS

NMR shows that some Na^+ ions are located in the Li layer that was not previously considered. It helped to reconsider the structural model used for the Rietveld refinement of the synchrotron XRD. This refinement led to the $\text{OP4-}[\text{Li}_{0.42}\text{Na}_{0.05}]\text{Na}_{0.32}\text{CoO}_2$ formula for the material. In addition, ^7Li and ^{23}Na MAS NMR provide information about the cationic mobility in the material. Up to 450 K no exchange has been observed for Li^+ ions at the NMR times scale whereas at room temperature, the ^{23}Na spectra reveals already a single average signal for Na ions in the prismatic sites (P layer) due to much larger ionic mobility. The lowest Li^+ ionic mobility compared to Na can be explained by different factors: i) a higher activation energy involved in the diffusion for the O-type layer, as the Li^+ has to go through a tetrahedral site to jump from an octahedra site to the adjacent one, whereas Na^+ can directly jump from the Na_e prismatic site to the Na_f one through a rectangular window. ii) a low amount of vacancies ($\sim 6\%$) in the Li O-type layers compared to vacancies in the P-type layer ($\sim 36\%$) and the presence of additional Na ($\sim 5\%$) in the Li layer.

Supporting Information

S1: Comparison of the crystallographic data for the different OP4 phases reported in literature. S2: SEM pictures of the sample A at different magnifications. S3: Representation of the different phases reported in this paper. S4: Experimental ^7Li MAS NMR spectra performed on a 7.05 T magnet with a spinning frequency of 30 kHz for 250 K, 300 K and 320 K. S5 : DFT calculation performed on a model $\text{Li}_{0.5}\text{Na}_{1/3}\text{CoO}_2$ cell : comparison between experimental NMR spectra and calculated ones, total and partial calculated spin DOS and 3D spin density map. S6: Experimental ^7Li SI spectra performed at 340 K with different mixing times. S7: Fitted parameters of the ^{23}Na MAS NMR spectra recorded while spinning at 13 kHz at variable temperatures.

The following files are available free of charge.

Corresponding author

*Email: dany.carlier@icmcb.cnrs.fr

Notes

The authors declare no competing financial interest.

Acknowledgments

This work beneficiates from financial support from the Fond Franco-Canadien pour la Recherche (FFCR). ALBA synchrotron is acknowledged for granting beamtime through proposal no 2017092426. We are also grateful to Mathieu Duttine for his technical support. The Mésocentre de Calcul Intensif Aquitain (MCIA) and the modelling center of ISM are acknowledged for computing facilities.

References

- (1) Hong, S. Y.; Kim, Y.; Park, Y.; Choi, A.; Choi, N.-S.; Lee, K. T. Charge Carriers in Rechargeable Batteries: Na Ions vs. Li Ions. *Energy Environ. Sci.* **2013**, *6* (7), 2067.
- (2) Kubota, K.; Komaba, S. Practical Issues and Future Perspective for Na-Ion Batteries. *J. Electrochem. Soc.* **2015**, *162* (14), A2538–A2550.
- (3) Lee, M.; Viciu, L.; Li, L.; Wang, Y.; Foo, M. L.; Watauchi, S.; Pascal Jr, R. A.; Cava, R. J.; Ong, N. P. Large Enhancement of the Thermopower in Na_xCoO_2 at High Na Doping. *Nat. Mater.* **2006**, *5* (7), 537–540.
- (4) Lee, M.; Viciu, L.; Li, L.; Wang, Y.; Foo, M. L.; Watauchi, S.; Pascal, R. A.; Cava, R. J.; Ong, N. P. Enhancement of the Thermopower in Na_xCoO_2 in the Large-X Regime ($x > 0.75$). *Phys. B Condens. Matter* **2008**, *403* (5–9), 1564–1568.
- (5) Takada, K.; Sakurai, H.; Takayama-Muromachi, E.; Izumi, F.; Dilanian, R. A.; Sasaki, T. Superconductivity in Two-Dimensional CoO_2 Layers. *Nature* **2003**, *422* (6927), 53–54.
- (6) Takada, K.; Fukuda, K.; Osada, M.; Nakai, I.; Izumi, F.; Dilanian, R. A.; Kato, K.; Takata, M.; Sakurai, H.; Takayama-Muromachi, E.; et al. Chemical Composition and Crystal Structure of Superconducting Sodium Cobalt Oxide Bilayer-Hydrate Electronic. *J. Mater. Chem.* **2004**, *14* (9), 1448.
- (7) Landron, S.; Soret, J.; Lepetit, M.-B. An *Ab Initio* Evaluation of the Local Effective Interactions in the Na_xCoO_2 Family. *J. Phys. Condens. Matter* **2010**, *22*, 1–8.
- (8) Delmas, C.; Fouassier, C.; Hagenmuller, P. Structural Classification and Properties of the Layered Oxides. *Phys. B C* **1980**, *99* (1–4), 81–85.
- (9) Lei, Y.; Li, X.; Liu, L.; Ceder, G. Synthesis and Stoichiometry of Different Layered Sodium Cobalt Oxides. *Chem. Mater.* **2014**, *26* (18), 5288–5296.
- (10) Levasseur, S.; Menetrier, M.; Suard, E.; Delmas, C. Evidence for Structural Defects in Non-Stoichiometric HT- LiCoO_2 : Electrochemical, Electronic Properties and ^7Li NMR Studies. *Solid State Ion.* **2000**, *128* (1–4), 11–24.
- (11) Carlier, D.; Croguennec, L.; Ceder, G.; Ménétrier, M.; Shao-Horn, Y.; Delmas, C. Structural Study of the $\text{T}^{\#2}\text{-Li}_x\text{CoO}_2$ ($0.52 < X \leq 0.72$) Phase. *Inorg. Chem.* **2004**, *43* (3), 914–922.
- (12) Braconnier, J.-J.; Delmas, C.; Fouassier, C.; Hagenmuller, P. Comportement Electrochimique Des Phases Na_xCoO_2 . *Mater. Res. Bull.* **1980**, *15* (12), 1797–1804.
- (13) Balsys, R. J.; Davis, R. L. The Structure of $\text{Li}_{0.43}\text{Na}_{0.36}\text{CoO}_{1.96}$ Using Neutron Powder Diffraction. *Solid State Ion.* **1994**, *69* (1), 69–74.
- (14) Berthelot, R.; Carlier, D.; Delmas, C. Electrochemical Investigation of the $\text{P2-Na}_x\text{CoO}_2$ Phase Diagram. *Nat. Mater.* **2011**, *10* (1), 74–80.
- (15) Ren, Z.; Shen, J.; Jiang, S.; Chen, X.; Feng, C.; Xu, Z.; Cao, G. Enhanced Thermopower in an Intergrowth Cobalt Oxide $\text{Li}_{0.48}\text{Na}_{0.35}\text{CoO}_2$. *J. Phys. Condens. Matter* **2006**, *18* (29), L379–L384.
- (16) Bos, J. W. G.; Hertz, J. T.; Morosan, E.; Cava, R. J. Magnetic and Thermoelectric Properties of Layered $\text{Li}_x\text{Na}_y\text{CoO}_2$. *J. Solid State Chem.* **2007**, *180* (11), 3211–3217.
- (17) Semenova, A.; Kellerman, D.; Baklanova, I.; Perelyaeva, L.; Vovkotrub, E. Raman Spectroscopy Study of Sodium–lithium Cobaltite. *Chem. Phys. Lett.* **2010**, *491* (4–6), 169–171.
- (18) Berthelot, R.; Pollet, M.; Carlier, D.; Delmas, C. Reinvestigation of the OP4-(Li/Na)CoO_2 -Layered System and First Evidence of the $(\text{Li/Na/Na})\text{CoO}_2$ Phase with OPP9 Oxygen Stacking. *Inorg. Chem.* **2011**, *50* (6), 2420–2430.
- (19) Kellerman, D. G.; Zhuravlev, N. A.; Semenova, A. S.; Shein, I. R.; Kuznetsov, M. V. ^{23}Na NMR in Binary Lithium–Sodium Cobaltite. *Bull. Russ. Acad. Sci. Phys.* **2011**, *75* (8), 1157–1159.

- (20) Mesilov, V. V.; Galakhov, V. R.; Semenova, A. S.; Kellerman, D. G.; Elokhina, L. V. X-Ray Spectra and Specific Features of the Structure of Lithium-Sodium Cobaltite $\text{Li}_x\text{Na}_y\text{CoO}_2$. *Phys. Solid State* **2011**, *53* (2), 271–275.
- (21) Yabuuchi, N.; Kawamoto, Y.; Hara, R.; Ishigaki, T.; Hoshikawa, A.; Yonemura, M.; Kamiyama, T.; Komaba, S. A Comparative Study of LiCoO_2 Polymorphs: Structural and Electrochemical Characterization of O2-, O3-, and O4-Type Phases. *Inorg. Chem.* **2013**, *52* (15), 9131–9142.
- (22) Grey, C. P.; Dupré, N. NMR Studies of Cathode Materials for Lithium-Ion Rechargeable Batteries. *Chem. Rev.* **2004**, *104* (10), 4493–4512.
- (23) Carlier, D.; Ménétrier, M.; Grey, C. P.; Delmas, C.; Ceder, G. Understanding the NMR Shifts in Paramagnetic Transition Metal Oxides Using Density Functional Theory Calculations. *Phys. Rev. B* **2003**, *67* (17).
- (24) Kim, J.; Middlemiss, D. S.; Chernova, N. A.; Zhu, B. Y. X.; Masquelier, C.; Grey, C. P. Linking Local Environments and Hyperfine Shifts: A Combined Experimental and Theoretical ^{31}P and ^7Li Solid-State NMR Study of Paramagnetic Fe(III) Phosphates. *J. American Chem. Soc.* **2010**, *132* (47), 16825–16840.
- (25) Mali, G.; Meden, A.; Dominko, R. ^6Li MAS NMR Spectroscopy and First-Principles Calculations as a Combined Tool for the Investigation of $\text{Li}_2\text{MnSiO}_4$ Polymorphs. *Chem. Commun.* **2010**, *46* (19), 3306–3308.
- (26) Castets, A.; Carlier, D.; Zhang, Y.; Boucher, F.; Marx, N.; Croguennec, L.; Ménétrier, M. Multinuclear NMR and DFT Calculations on the $\text{LiFe}(\text{PO}_4)\text{OH}$ and $\text{Fe}(\text{PO}_4)\text{H}_2\text{O}$ Homeotypic Phases. *J. Phys. Chem. C* **2011**, *115*, 16234–16241.
- (27) Zhang, Y.; Castets, A.; Carlier, D.; Ménétrier, M.; Boucher, F. Simulation of NMR Fermi Contact Shifts for Lithium Battery Materials: The Need for an Efficient Hybrid Functional Approach. *J. Phys. Chem. C* **2012**, *116* (33), 17393–17402.
- (28) Clément, R. J.; Xu, J.; Middlemiss, D. S.; Alvarado, J.; Ma, C.; Meng, Y. S.; Grey, C. P. Direct Evidence for High Na^+ Mobility and High Voltage Structural Processes in $\text{P2-Na}_x[\text{Li}_y\text{Ni}_z\text{Mn}_{1-y-z}]\text{O}_2$ ($X, Y, Z \leq 1$) Cathodes from Solid-State NMR and DFT Calculations. *J. Mater. Chem. A* **2017**, *5* (8), 4129–4143.
- (29) Castets, A.; Carlier, D.; Zhang, Y.; Boucher, F.; Ménétrier, A DFT-Based Analysis of the NMR Fermi Contact Shifts in Tavorite-like $\text{LiMPO}_4\text{-OH}$ and $\text{MPO}_4\text{-H}_2\text{O}$ ($M = \text{Fe, Mn, V}$). *J. Phys. Chem. C* **2012**, *116* (34), 18002–18014.
- (30) Bamine, T.; Boivin, E.; Boucher, F.; Messinger, R. J.; Salager, E.; Deschamps, M.; Masquelier, C.; Croguennec, L.; Ménétrier, M.; Carlier, D. Understanding Local Defects in Li-Ion Battery Electrodes through Combined DFT/NMR Studies: Application to LiVPO_4F . *J. Phys. Chem. C* **2017**, *121* (6), 3219–3227.
- (31) Nguyen, L. H.; Sanz Camacho, P.; Broux, T.; Olchowka, J.; Masquelier, C.; Croguennec, L.; Carlier, D. Density Functional Theory-Assisted ^{31}P and ^{23}Na Magic-Angle Spinning Nuclear Magnetic Resonance Study of the $\text{Na}_3\text{V}_2(\text{PO}_4)_2\text{F}_3\text{-Na}_3\text{V}_2(\text{PO}_4)_2\text{FO}_2$ Solid Solution: Unraveling Its Local and Electronic Structures. *Chem. Mater.* **2019**, *31* (23), 9759–9768.
- (32) Cahill, L. S.; Chapman, R. P.; Kirby, C. W.; Goward, G. R. The Challenge of Paramagnetism in Two-Dimensional $^6, ^7\text{Li}$ Exchange NMR. *Appl. Magn. Reson.* **2007**, *32* (4), 565–581.
- (33) Davis, L. J. M.; Heinmaa, I.; Goward, G. R. Study of Lithium Dynamics in Monoclinic $\text{Li}_3\text{Fe}_2(\text{PO}_4)_3$ Using ^6Li VT and 2D Exchange MAS NMR Spectroscopy. *Chem. Mater.* **2010**, *22* (3), 769–775.
- (34) Cahill, L. S.; Chapman, R. P.; Britten, J. F.; Goward, G. R. ^7Li NMR and Two-Dimensional Exchange Study of Lithium Dynamics in Monoclinic $\text{Li}_3\text{V}_2(\text{PO}_4)_3$. *J. Phys. Chem. B* **2006**, *110* (14), 7171–7177.
- (35) Cahill, L. S.; Kirby, C. W.; Goward, G. R. $^6\text{Li}\{^{31}\text{P}\}$ Rotational-Echo, Double-Resonance Studies of Lithium Ion Site Dynamics in $\text{Li}_3\text{V}_2(\text{PO}_4)_3$. *J. Phys. Chem. C* **2008**, *112* (6), 2215–2221.

- (36) Smiley, D. L.; Davis, L. J. M.; Goward, G. R. An Improved Understanding of Li⁺ Hopping Pathways and Rates in Li₃Fe₂(PO₄)₃ Using Selective Inversion ⁶Li NMR Spectroscopy. *J. Phys. Chem. C* **2013**, *117* (46), 24181–24188.
- (37) Rodríguez-Carvajal, J. Recent Advances in Magnetic Structure Determination by Neutron Powder Diffraction. *Phys. B Condens. Matter* **1993**, *192* (1–2), 55–69.
- (38) Massiot, D.; Fayon, F.; Capron, M.; King, I.; Le Calvé, S.; Alonso, B.; Durand, J.-O.; Bujoli, B.; Gan, Z.; Hoatson, G. Modelling One-and Two-Dimensional Solid-State NMR Spectra. *Magn. Reson. Chem.* **2002**, *40* (1), 70–76.
- (39) Bielecki, A.; Burum, D. P. Temperature Dependence of ²⁰⁷Pb MAS Spectra of Solid Lead Nitrate. An Accurate, Sensitive Thermometer for Variable-Temperature MAS. *J. Magn. Reson. A* **1995**, *116* (2), 215–220.
- (40) Takahashi, T.; Kawashima, H.; Sugisawa, H.; Baba, T. ²⁰⁷Pb Chemical Shift Thermometer at High Temperature for Magic Angle Spinning Experiments. *Solid State Nucl. Magn. Reson.* **1999**, *15* (2), 119–123.
- (41) Ganguly, P.; Ramaswamy, V.; Mulla, I. S.; Shinde, R. F.; Bakare, P. P.; Ganapathy, S.; Rajamohanam, P. R.; Prakash, N. V. K. Application of a Layered Triangular-Lattice Magnetic Model System to LiNiO₂. *Phys. Rev. B* **1992**, *46*, 11595. <https://doi.org/doi.org/10.1103/PhysRevB.46.11595>.
- (42) Alcantara, R.; Lavela, P.; Tirado, J. L.; Zhecheva, E.; Stoyanova, R. SPES, ⁶Li MAS NMR, and Ni³⁺ EPR Evidence for the Formation of Co²⁺-Containing Spinel Phases in LiCoO₂ Cycled Electrode Materials. *J. Electroanal. Chem.* **1998**, *454* (1–2), 173–181.
- (43) Peeters, M. P. J.; Van Bommel, M. J.; Neilen-ten Wolde, P. M. C.; Van Hal, H. A. M.; Keur, W. C.; Kentgens, A. P. M. A ⁶Li, ⁷Li and ⁵⁹Co MAS NMR Study of Rock Salt Type Li_xCoO₂ (0.48 ≤ x ≤ 1.05). *Solid State Ion.* **1998**, *112* (1–2), 41–52. [https://doi.org/doi.org/10.1016/S0167-2738\(98\)00213-6](https://doi.org/doi.org/10.1016/S0167-2738(98)00213-6).
- (44) Ménétrier, M.; Saadouné, I.; Lévassé, S.; Delmas, C. The Insulator-Metal Transition upon Lithium Deintercalation from LiCoO₂: Electronic Properties and ⁷Li NMR Study. *J. Mater. Chem.* **1999**, *9* (5), 1135–1140.
- (45) Takahata, K.; Iguchi, Y.; Tanaka, D.; Itoh, T.; Terasaki, I. Low Thermal Conductivity of the Layered Oxide (Na,Ca)Co₂O₄: Another Example of a Phonon Glass and an Electron Crystal. *Phys. Rev. B* **2000**, *61* (19), 12551.
- (46) Motohashi, T.; Naujalis, E.; Ueda, R.; Isawa, K.; Karppinen, M.; Yamauchi, H. Simultaneously Enhanced Thermoelectric Power and Reduced Resistivity of Na_xCo₂O₄ by Controlling Na Nonstoichiometry. *Appl. Phys. Lett.* **2001**, *79* (10), 1480–1482.
- (47) Pan, C.; Lee, Y. J.; Amundsen, B.; Grey, C. P. ⁶Li MAS NMR Studies of the Local Structure and Electrochemical Properties of Cr-Doped Lithium Manganese and Lithium Cobalt Oxide Cathode Materials for Lithium-Ion Batteries. *Chem. Mater.* **2002**, *14* (5), 2289–2299.
- (48) Aykol, M.; Kim, S.; Wolverton, C. Van Der Waals Interactions in Layered Lithium Cobalt Oxides. *J. Phys. Chem. C* **2015**, *119* (33), 19053–19058. <https://doi.org/10.1021/acs.jpcc.5b06240>.
- (49) Hinuma, Y.; Meng, Y. S.; Ceder, G. Temperature-Concentration Phase Diagram of P2 Na_xCoO₂ from First-Principles Calculations. *Phys. Rev. B* **2008**, *77* (22).
- (50) Van der Ven, A.; Aydinol, M. K.; Ceder, G.; Kresse, G.; Hafner, J. First-Principles Investigation of Phase Stability in Li_xCoO₂. *Phys. Rev. B* **1998**, *58* (6), 2975–2987.
- (51) Platova, T. A.; Mukhamedshin, I. R.; Alloul, H.; Dooglav, A. V.; Collin, G. Nuclear Quadrupole Resonance and X-Ray Investigation of the Structure of Na_{2/3}CoO₂. *Phys. Rev. B* **2009**, *80* (22).
- (52) Carlier, D.; Blangero, M.; Ménétrier, M.; Pollet, M.; Doumerc, J.-P.; Delmas, C. Sodium Ion Mobility in Na_xCoO₂ (0.6 < X < 0.75) Cobaltites Studied by ²³Na MAS NMR. *Inorg. Chem.* **2009**, *48* (15), 7018–7025.

- (53) Carlier, D.; Cheng, J. H.; Berthelot, R.; Guignard, M.; Yoncheva, M.; Stoyanova, R.; Hwang, B. J.; Delmas, C. The P2-Na_{2/3}Co_{2/3}Mn_{1/3}O₂ Phase: Structure, Physical Properties and Electrochemical Behavior as Positive Electrode in Sodium Battery. *Dalton Trans.* **2011**, 40 (36), 9306.
- (54) Singh, G.; Lopez Del Amo, J. M.; Galceran, M.; Perez-Villar, S.; Rojo, T. Structural Evolution during Sodium Deintercalation/intercalation in Na_{2/3}[Fe_{1/2}Mn_{1/2}]O₂. *J. Mater. Chem. A* **2015**, 3 (13), 6954–6961.
- (55) Guignard, M.; Carlier, D.; Didier, C.; Suchomel, M.; Elkäim, E.; Bordet, P.; Decourt, R.; Darriet, J.; Delmas, C. Vanadium Clustering/Declustering in P2–Na_{1/2}VO₂ Layered Oxide. *Chem. Mater.* **2014**, 26 (4), 1538–1548.

For Table of Contents Only

The local structure, electronic structure and dynamics of the original OP4-(Li/Na)CoO₂ phase were studied by ⁷Li and ²³Na MAS NMR. ⁷Li NMR showed that NMR shifts result from two contributions: the Fermi contact and the Knight shifts and indicate the presence of Co ions with different local electronic structures. ²³Na NMR showed that some Na⁺ ions are located in the Li layer and that Na⁺ ions are more mobile than Li⁺ ones at RT.

